In situ structure and assembly of the multidrug efflux pump AcrAB-TolC

Xiaodong Shi[1,2]†, Muyuan Chen[1]†, Zhili Yu[1], James M. Bell[1,3], Hans Wang[1], Isaac Forrester[4], Heather Villarreal[4], Joanita Jakana[4], Dijun Du[5,6#], Ben F. Luisi[5], Steven J. Ludtke[1] & Zhao Wang[1,7*]

[1]Verna and Marrs McLean Department of Biochemistry and Molecular Biology, Baylor College of Medicine, Houston, Texas 77030, USA.

[2]Jiangsu Province Key Laboratory of Anesthesiology and Jiangsu Province Key Laboratory of Anesthesia and Analgesia Application, Xuzhou Medical University, Xuzhou, Jiangsu 221004, China.

[3]Graduate Program in Quantitative and Computational Biosciences, Baylor College of Medicine, Houston, Texas 77030, USA.

[4]CryoEM Core at Baylor College of Medicine, Houston, Texas 77030, USA.

[5] Department of Biochemistry, University of Cambridge, Cambridge CB21GA, UK.

[6] School of Life Science and Technology, ShanghaiTech University, Shanghai 201210, China.

[7]Department of Molecular and Cellular Biology, Baylor College of Medicine, Houston, Texas 77030, USA.

†These authors contributed equally to this work.

[#]Current address.

*Corresponding author. Email: zhaow@bcm.edu.

Abstract

Multidrug efflux pumps actively expel a wide range of toxic substrates from the cell and play a major role in intrinsic and acquired drug resistance. In Gram-negative bacteria, these pumps form tripartite assemblies that span the cell envelope. However, the in situ structure and assembly mechanism of multidrug efflux pumps remain unknown. Here we report the in situ structure of the *Escherichia coli* AcrAB-TolC multidrug efflux pump obtained by electron cryo-tomography and subtomogram averaging. The fully assembled efflux pump is observed in a closed state under conditions of antibiotic challenge and in an open state in the presence of AcrB inhibitor. We also observe intermediate AcrAB complexes without TolC and discover that AcrA contacts the peptidoglycan layer of the periplasm. Our data point to a sequential assembly process in living bacteria, beginning with formation of the AcrAB subcomplex and suggest domains to target with efflux pump inhibitors.

Introduction

With the increasing use of antibiotics, multidrug resistance in pathogenic bacteria has become a public health crisis. The capability of numerous bacterial species to survive in the presence of antibiotics and toxic compounds is partially conferred by the activity of energy-dependent efflux pumps[1,2]. In Gram-negative bacteria, these pumps are multicomponent assemblies that span the cell envelope and are driven by a primary or a secondary transport component located in the inner membrane[3]. AcrAB-TolC is one of the tripartite pumps that are constitutively expressed in *Escherichia coli* (*E. coli*)[4,5]. As the main multidrug efflux machinery, AcrAB-TolC is comprised of the outer membrane protein TolC, the periplasmic adaptor protein AcrA, and the inner membrane transporter AcrB from the Resistance-Nodulation-cell Division (RND) superfamily[3]. The AcrAB-TolC efflux pump transports diverse compounds, conferring resistance to a broad spectrum of antibiotics[6]. Structural studies of this pump have been limited to individual components by X-ray crystallography[7-14] or fully assembled pumps by cryo-electron microscopy (cryo-EM) single particle analysis[15-19]. These approaches revealed structures in vitro, but the in situ structure of this pump remains unknown. Due to the dynamic nature of the three components and their low binding affinities, it is particularly challenging to capture the intermediate states of the AcrAB-TolC pump in vitro, and there is only limited information about the assembly mechanism of the pump in living cells. Here, we visualize the in situ structure of *E. coli* AcrAB-TolC efflux pump by employing cellular electron cryo-tomography (cryo-ET) and subtomogram averaging. Our results reveal in situ structures of the fully assembled pump and its intermediate assembly state and suggest an assembly mechanism for tripartite efflux pumps in Gram-negative bacteria.

Results

Visualization of AcrAB-TolC pump in *E. coli* cell envelope

To enrich AcrAB-TolC pumps in situ, we overexpressed AcrA, AcrB, and TolC in BL21 (DE3) cells at a level at which the cells can still replicate and grow (Supplementary Figure 1). Then we imaged cells with Cryo-ET under antibiotic treatment that promotes pump assembly[20]. Three-dimensional tomographic reconstructions revealed detailed structures of the Gram-negative bacterial envelope, with abundant channel-like densities spanning the cell envelope (Fig. 1 and Supplementary Movie 1). These densities are rarely observed in wild type *E. coli* cells

(Supplementary Figure 2), implying that they correspond to AcrAB-TolC pumps. In addition, the distance between the outer membrane and the inner membrane stays constant at the sites where the AcrAB-TolC pumps occur, suggesting that the periplasm may be pinched by these assemblies.

In situ structures of the fully assembled AcrAB-TolC complex

In order to determine the in situ structure of AcrAB-TolC pump, we extracted particles of the cell envelope spanning densities and performed subtomogram averaging. From 1,321 subtomograms of the AcrAB-TolC pump with C3 symmetry, we achieved a reconstruction at ~15 Å resolution (gold standard FSC, see methods) (Supplementary Figure 3 and Supplementary Figure 4). The averaged map resembles the EM structure of the AcrAB-TolC pump, with a length of ~33 nm (Fig. 2a-c). The in situ arrangement of each component of the pump matches the previous cryo-EM studies[15-17]. The overall architecture of the fully assembled pump clearly indicates a 3:6:3 ratio for TolC: AcrA: AcrB in situ (Fig. 2b-c), which agrees with our previous cryo-EM structures[16,19]. Notably, the density occupancy in the TolC region is considerably lower than the rest of the structure, suggesting that TolC may be absent in a subset of the particles (Supplementary Figure 5a). We then performed focused classification with a soft spherical mask on the upper part of the pump (Supplementary Figure 5b). This classification yielded two maps, one showing the full pump with a visible TolC density, and the other one containing only the AcrAB subassembly of the pump and the density of the cell membranes (Supplementary Figure 5c and Supplementary Figure 6).

In the fully assembled pump, the inner chamber shows a clear constriction (Fig. 2a, c), which has only been observed in the apo-form of an AcrA-AcrB crosslinked pump in previous in vitro experiments[19]. Therefore, we concluded that the map corresponded to a closed state and it fitted our higher resolution published structure (PDB: 5V5S) well. Despite the presence of the antibiotic, we did not capture the transporting state where a continuous conduit is formed between TolC and AcrA. However, our drug resistance test showed that the strain overexpressing the AcrAB-TolC pumps had a much higher minimum inhibitory concentration (MIC) than the wild-type strain (Supplementary Table 1), indicating that the AcrAB-TolC pumps are functional. Thus, there must be pumps that are in a transporting state in the bacteria, in order

to produce the antibiotic resistance. To validate that the AcrAB-TolC pumps can open in our system, we treated the cells with MBX3132, an inhibitor of AcrB, that is known to lock AcrB of the pump in vitro[19]. According to our MIC results, both the wild-type strain and the AcrAB-TolC pump overexpressing strain became hyper-resistant to puromycin in the presence of MBX3132 (Supplementary Table 1). Using the same data collection and processing protocol, we captured the open state pump that had a continuous conduit through TolC and AcrA. The structure has a length of 32 nm, shorter than that of closed state (Fig. 2d and Supplementary Figure 7), consistent with our in vitro results obtained by cryo-EM[19]. The data indicate that contraction along the long axis is part of active transport in vivo. Taken together, our data suggest that the opening of the pump and efflux of antibiotics is likely a transient process, with the majority of the complexes observed at any given time in a closed state, rather than an active state.

Compared to single particle cryo-EM, cellular Cryo-ET provides the capability of visualizing the interactions of a protein complex with its surroundings. In the tomograms of bacteria under antibiotic pressure, we found that the density of the PG layer is situated just above the top of AcrA when the cell envelope densities are overlaid with the averaged map of the full pump (Fig. 2e). These observations suggest that the PG is contacted both by the coiled-coils of TolC and the α-hairpin loop of AcrA, instead of the equatorial domain of TolC as previously proposed[21]. These interactions are validated by the mask-free subtomogram average of the same particles (Supplementary Figure 8). In addition, our in vivo crosslinking experiment mapped the binding sites of both AcrA and TolC with PG (Supplementary Figure 9 and Supplementary Figure 10), further verifying our observation that both AcrA and TolC interact with PG in the complex.

In situ structure of the AcrAB subcomplex

As mentioned above, the three-dimension classification of subtomograms revealed ~38% of the particles within the dataset do not have TolC located in the outer membrane (see Methods). The averaged density map of these particles represents a bipartite AcrAB subcomplex (Fig. 3a-c), in which the quaternary organization of AcrA and AcrB is similar to a proposed assembly model based on the crystal structure of the recombinant heavy-metal efflux pump CusBA[22]. In the structure of AcrAB subcomplex, six protruding densities of AcrA in the averaged map indicate a 6:3 ratio between AcrA and AcrB, the same as the fully assembled pump (Supplementary Figure

5c). The interior of AcrA viewed in a cross-section through the averaged map of the subcomplex differs from that of the fully assembled pump, with the chamber inside AcrA being smaller (Fig. 3c) and the AcrA hairpin domains not forming a complete ring structure (Supplementary Figure 5c). The helical hairpin region of AcrA repacks to form an alpha-helical barrel in the transition from the apo to the ligand-bound states of the AcrAB-TolC assembly, and the reorganization of the AcrA hexamer is likely to be a critical step for the opening of the TolC channel to form the active tripartite pump complex[19].

In the unmasked average, the tip of AcrA density merges into the density of PG layer, while the space between the PG and the outer membrane is empty (Fig. 3d). The PG layer possibly serves as an anchor to hold the AcrA hexamer in the periplasm to maintain the stability of AcrAB subcomplex in the envelope or to help the bipartite AcrAB subcomplex recruit TolC. Our finding that the AcrAB subcomplex exists as a stable entity in cells is supported by previous experiments both in vivo and in vitro[20,23,24]. We did not observe any complex directly between AcrB and TolC, which is consistent with prior structural studies[15,16,19]. Likewise, AcrA-TolC complexes were not detected in cells either.

Discussion

In conclusion, we suggest that the pump assembly process follows a sequential order. Based on the tomography results and data from in vivo interactions, it is likely that AcrB and AcrA can associate to form a bipartite complex. The contact between the α-hairpin domain of AcrA and PG helps to position and maintain the stability of the AcrAB complex in the cell envelope, and may permit the subcomplex to walk along the layer until it encounters TolC (Fig. 4). In the presence of antibiotics, the AcrAB subcomplex changes its conformation to recruit TolC, which remains closed in the outer membrane to keep the periplasm isolated from the extracellular environment. Notably, the in situ fully assembled closed state pump showed a constriction in between TolC and AcrA. Next, the pump briefly adopts an open conformation accompanied with a contraction to promote the expulsion of the substrate through the chamber and closes immediately after the drug molecule is expelled.

In this study, we captured the fully assembled pumps on *E. coli* membranes exhibiting a closed

state in the presence of antibiotics and an open state in the presence of the AcrB inhibitor. In contrast, the structures determined from purified samples are always in an open state in the presence of antibiotic or inhibitor[19]. The significant difference between in situ and in vitro structures suggests that the OM-PG-IM envelope structure in Gram-negative bacteria and the potential between the two sides of the inner membrane may be essential for the regulation of drug efflux by keeping the conformational changes of TolC and AcrA coupled with the substrate binding of AcrB. In the cellular environment, AcrA has its N-terminal anchored in the inner membrane and the its α-hairpin contacting PG, communicating between AcrB and TolC to regulate the closing and opening of the pump. Such association is disrupted during the purification, resulting in the constantly open AcrAB-TolC pump. In addition, the observation of AcrAB subcomplex suggests a critical role of PG in the assembly of the pump, which is not preserved in the purified system. With this insight, we propose that interfering with the interactions of AcrA with the PG or AcrB may interrupt the assembly process and block the function of the tripartite efflux pumps, suggesting an approach to therapeutics targeting assembly.

Our results provide the first structure of the AcrAB-TolC pump and its intermediate assembly state in the native cell membrane environment. This shows the potential of in situ membrane protein structure determination with Cryo-ET. While single particle analysis has shown great success in solving detailed protein structures, significant efforts are still needed for membrane protein purification, and the resulting structures may not truly represent their native state. The recent developments in cryo-ET make it possible to determine 10-20 Å resolution structures of membrane embedded molecular machines[25,26], and resolve their compositional and conformational variability in the native environment.

Methods

Plasmid construction and protein expression. Plasmid pAcBH which carries the *acrAB* locus and coexpresses AcrA and His-tagged AcrB was a gift from Dr. Akihito Yamaguchi (Osaka University, Suita, Japan)[27]. The *tolC* gene was first amplified using primers TolCinf_F: 5′-AAGGAGATATACATATGAAGAAATTGCTCCCCATTCTTATCGGCC-3′ and TolCFLAGXhoI_R: 5′-GAGCTCGAGTCACTTATCGTCGTCATCCTTGTAATCGTTACGGAAAGGGTTATGACC

GTTACTGGT-3′, and then was amplified again using TolCinf_F and TolCFLAG_inf_R: 5′-TTGAGATCTGCCATATGTCACTTATCGTCGTCATCCTTGTAATCGTTACG-3′. The resulting DNA fragment of *tolC-FLAG* was cloned into the pRSFDuet-1 plasmid using the In-Fusion cloning method, yielding pRSFDuet-*tolC*. *E. coli* BL21 (DE3) cells (Invitrogen) were co-transformed with plasmids pAcBH and pRSFDuet-*tolC* to overexpress AcrAB-TolC pump. Cells were cultured in 2xYT medium with 100 μg/ml ampicillin and 50 μg/ml kanamycin at 37 ^{o}C until an OD_{600} of 0.8 was reached and then induced by addition of 0.1 mM isopropyl 1-thio-β-D-galactopyranoside (IPTG) at 20 ^{o}C overnight. Protein expression was examined by Coomassie blue staining and western blotting analysis.

Minimum inhibitory concentration. Minimum inhibitory concentration (MIC) of puromycin was measured by the twofold dilution method as described previously with minor modifications[28]. Briefly, exponentially growing cultures (OD_{600} of 0.8) were inoculated at a density of 10^4 cells per ml into LB medium containing appropriate antibiotics in the presence of two-fold increasing concentrations of puromycin. Cell growth was determined visually after incubation at 37 ^{o}C for 20 h.

In vivo crosslinking and LC/MS-MS analysis. *E. coli* strain C43 (DE3) delta *acrAB* was co-transformed with plasmid pET20b co-expressing AcrA S273C and AcrB S258C[19] and pRSF-duet co-expressing AcrZ and TolC. The S->C point mutations form a stabilising disulfide bridge between AcrA and AcrB. Cells were grown in 2xYT medium with 50 μg/ml carbenicillin and 50 μg/ml kanamycin at 37 ^{o}C to OD_{600} of 0.5 and then induced with 1 mM IPTG. After 2 h, cells were harvested by spinning at 4000 g for 5 min, then resuspended in phosphate buffered saline (PBS) supplemented with 0.2% wt/vol glucose. In vivo crosslinking of proteins to the peptidoglycan with the bifunctional 3,3'-dithiobis (sulfosuccinimidyl proprionate) (DTSSP) and isolation of the peptidoglycan with sodium dodecylsulfate followed the protocol of Li and Howard[29], with modifications. A control sample was also prepared without crosslinking. The isolated peptidoglycan from the samples were washed three times with PBS to remove traces of sodium dodecylsulfate, then incubated in PBS with 2 mg/ml lysozyme for 30 min at 37 ^{o}C to digest the peptidoglycan. The samples were centrifuged at 12000 g for 10 min and the supernatants loaded onto a 4-12% gradient denaturing PAGE gel without reducing agent and

stained with Coomassie brilliant blue G. A band at roughly 80 kDa that was not present in the control was excised from the gel, treated with DTT to reduce the DTSSP and then digested with chymotrypsin and analysed by LC/MS-MS by the University of Cambridge Proteomics Facility. TolC was identified with an emPAI score of 11.1 and AcrA with a score of 10.2. Controls with bovine serum albumin (BSA) were also analysed from the same gel, selecting a band that migrated as a dimer. The crosslinked BSA sample identified 126 peptides that had reacted with the DTSSP, while the control showed 4 false positives. The location of the peptide fragments with mass corresponding to reduced DTSSP were mapped onto the crystal structures of TolC and AcrA and correspond to the equatorial domain and helical hairpin of TolC and the helical hairpin, lipoyl domain and membrane proximal domain of AcrA (see Supplementary Figure 9 and Supplementary Figure 10).

Cryo-ET sample preparation. *E. coli* cells were harvested and washed by PBS buffer, then resuspended to an OD_{600} of 1.0. Cultures were mixed with puromycin (600 μg/ml) or MBX3132 (1.4 μg/ml) and incubated at 37 ^{o}C for half an hour. Subsequently, cells were mixed with a solution of 10 nm BSA fiducial gold (Aurion) immediately before freezing in a 1:3 cell solution to BSA gold fiducial. A single 3 μl droplet of the sample was applied to the freshly glow-discharged, continuous floating carbon film covered grids (Quantifoil Au R3.5/1, 200 mesh) and plunge frozen using a Vitrobot Mark IV (FEI). Grids were stored in liquid nitrogen until required for data collection.

Cryo-ET data collection and 3D reconstructions. The frozen-hydrated samples were imaged on a JEOL 3200FSC (JEOL) operated at 300 kV using a K2 Summit direct electron detector camera (GATAN), with a magnification of 10,000x for antibiotic treated cells and 12,000x for MBX3132 treated cells. The pixel size is calibrated to be 3.366 Å and 2.75 Å, respectively. SerialEM[30] was used to collect low-dose, single-axis tilt series at -3 to -6 μm defocus range with an average cumulative dose of ~76 e−/Å^2 distributed over 33 images and covering an angular range of -50^{o} to +50^{o}, with an angular increment of 3^{o}. Tilted images were automatically aligned and reconstructed using EMAN2 software[31,32]. In total, more than 70 tomograms were generated to provide a sufficient selection for further processing. Supplementary Table 2 summarizes the Cryo-ET data analysis and validation statistics.

Subtomogram averaging and correspondence analysis. 25 high SNR particles were used for initial model generation. A two-step approach was used to build the initial model. First 5 iterations of the EMAN2 initial model generation routine were performed imposing C1 symmetry. After aligning the result to the symmetry axis, we performed 5 more iterations with C3 symmetry, and used the resulting map as the initial model for subtomogram refinement. Subtomogram averaging was then performed using 1,321 particles from 9 tomograms while applying C3 symmetry. This map was then used as the initial model for the following subtomogram refinement. To focus on the protein while preserving information from the membrane for improved alignment, a mask with values ranging from 0.5-1 around the pump and 0-0.5 covering a larger cylinder (~270 Å) was used for the iterative subtomogram refinement (see Supplementary Figure 11). The refinement is performed in a gold-standard fashion with all particles split into two subsets and resolution is measured by the Fourier shell correlation of the density maps from the two subsets. After 3 iteration of subtomogram refinement, a 19 Å resolution averaged structure was achieved.

As described in the main text, the TolC region in the averaged map has lower occupancy. For further classification, we used a soft spherical mask covering the TolC region. Two initial models were generated from the averaged map obtained from the last step, one with 0.5x intensity value while the other has 1.5x intensity value inside the mask. The two maps are identical outside the mask. The two maps were used to seed a focused classification under the spherical mask for 5 iterations, resulting in two classes of particles and their corresponding density maps (see Supplementary Figure 5).

The two classes of particles are then subject to 3 iterations of subtomogram refinement separately, using their corresponding initial model and the same mask. The subtomogram refinement is followed by 3 iterations of sub-tilt refinement, which produced the two structures shown in the figures.

To solve the structure of the pump with inhibitor, 678 particles from 10 tomograms are used for subtomogram averaging. The same initial model from the previous dataset was filtered to 50 Å

and used as the initial model for the subtomogram averaging. The 21 Å structure shown in the figure was achieved after 3 iterations of subtomogram refinement.

Visualization and model docking is performed in UCSF Chimera[33] and the built-in fit in map tool.

Data availability

The authors declare that all data supporting the findings of this study are available within the paper and its supplementary information files. The source data underlying Supplementary Figs 1a is provided as a Source Data file. Raw data for the chemical cross-links (source data for Supplementary Figure 9 and Supplementary Figure 10) is available via Zenodo data repository with a DOI (10.5281/zenodo.2656660). The cryo-ET structure of the AcrAB subcomplex, AcrAB-TolC close state and AcrAB-TolC open state were deposited in the EMDB under ID codes EMD-0531, EMD-0532 and EMD-0533, respectively. Raw cryo-ET data are available from the corresponding author upon reasonable request. Software scripts used in this data analyses are included within EMAN2 package which is available for download.

References

1. Poole, K. Efflux-mediated antimicrobial resistance. *J. Antimicrob. Chemother.* **56**, 20–51 (2005).
2. Li, X.-Z., Plésiat, P. & Nikaido, H. The challenge of efflux-mediated antibiotic resistance in Gram-negative bacteria. *Clin. Microbiol. Rev.* **28**, 337–418 (2015).
3. Du, D., van Veen, H. W., Murakami, S., Pos, K. M. & Luisi, B. F. Structure, mechanism and cooperation of bacterial multidrug transporters. *Curr. Opin. Struct. Biol.* **33**, 76–91 (2015).
4. Ma, D. *et al.* Genes acrA and acrB encode a stress-induced efflux system of Escherichia coli. *Mol. Microbiol.* **16**, 45–55 (1995).
5. Nikaido, H. Multidrug resistance in bacteria. *Annu. Rev. Biochem.* **78**, 119–146 (2009).
6. Okusu, H., Ma, D. & Nikaido, H. AcrAB efflux pump plays a major role in the antibiotic resistance phenotype of Escherichia coli multiple-antibiotic-resistance (Mar) mutants. *J. Bacteriol.* **178**, 306–308 (1996).
7. Koronakis, V., Sharff, A., Koronakis, E., Luisi, B. & Hughes, C. Crystal structure of the bacterial membrane protein TolC central to multidrug efflux and protein export. *Nature* **405**, 914–919 (2000).
8. Mikolosko, J., Bobyk, K., Zgurskaya, H. I. & Ghosh, P. Conformational flexibility in the multidrug efflux system protein AcrA. *Structure* **14**, 577–587 (2006).

9. Eicher, T. *et al.* Transport of drugs by the multidrug transporter AcrB involves an access and a deep binding pocket that are separated by a switch-loop. *Proc. Natl. Acad. Sci. U.S.A.* **109**, 5687–5692 (2012).
10. Murakami, S., Nakashima, R., Yamashita, E. & Yamaguchi, A. Crystal structure of bacterial multidrug efflux transporter AcrB. *Nature* **419**, 587–593 (2002).
11. Murakami, S., Nakashima, R., Yamashita, E., Matsumoto, T. & Yamaguchi, A. Crystal structures of a multidrug transporter reveal a functionally rotating mechanism. *Nature* **443**, 173–179 (2006).
12. Seeger, M. A. *et al.* Structural asymmetry of AcrB trimer suggests a peristaltic pump mechanism. *Science* **313**, 1295–1298 (2006).
13. Sennhauser, G., Amstutz, P., Briand, C., Storchenegger, O. & Grütter, M. G. Drug export pathway of multidrug exporter AcrB revealed by DARPin inhibitors. *PLoS Biol.* **5**, e7 (2007).
14. Sjuts, H. *et al.* Molecular basis for inhibition of AcrB multidrug efflux pump by novel and powerful pyranopyridine derivatives. *Proc. Natl. Acad. Sci. U.S.A.* **113**, 3509–3514 (2016).
15. Daury, L. *et al.* Tripartite assembly of RND multidrug efflux pumps. *Nat Commun* **7**, 10731 (2016).
16. Du, D. *et al.* Structure of the AcrAB-TolC multidrug efflux pump. *Nature* **509**, 512–515 (2014).
17. Jeong, H. *et al.* Pseudoatomic Structure of the Tripartite Multidrug Efflux Pump AcrAB-TolC Reveals the Intermeshing Cogwheel-like Interaction between AcrA and TolC. *Structure* **24**, 272–276 (2016).
18. Kim, J.-S. *et al.* Structure of the tripartite multidrug efflux pump AcrAB-TolC suggests an alternative assembly mode. *Mol. Cells.* **38**, 180–186 (2015).
19. Wang, Z. *et al.* An allosteric transport mechanism for the AcrAB-TolC multidrug efflux pump. *Elife* **6**, (2017).
20. Tikhonova, E. B. & Zgurskaya, H. I. AcrA, AcrB, and TolC of Escherichia coli Form a Stable Intermembrane Multidrug Efflux Complex. *J. Biol. Chem.* **279**, 32116–32124 (2004).
21. Meroueh, S. O. *et al.* Three-dimensional structure of the bacterial cell wall peptidoglycan. *Proc. Natl. Acad. Sci. U.S.A.* **103**, 4404–4409 (2006).
22. Su, C.-C. *et al.* Crystal structure of the CusBA heavy-metal efflux complex of Escherichia coli. *Nature* **470**, 558–562 (2011).
23. Zgurskaya, H. I. & Nikaido, H. Cross-linked complex between oligomeric periplasmic lipoprotein AcrA and the inner-membrane-associated multidrug efflux pump AcrB from Escherichia coli. *J. Bacteriol.* **182**, 4264–4267 (2000).
24. Touzé, T. *et al.* Interactions underlying assembly of the Escherichia coli AcrAB-TolC multidrug efflux system. *Mol. Microbiol.* **53**, 697–706 (2004).
25. Hu, B., Lara-Tejero, M., Kong, Q., Galán, J. E. & Liu, J. In Situ Molecular Architecture of the Salmonella Type III Secretion Machine. *Cell* **168**, 1065-1074.e10 (2017).
26. Rapisarda, C. *et al*. In situ and high-resolution cryo-EM structure of a bacterial type VI secretion system membrane complex. *EMBO J*. doi:10.15252/embj.2018100886 (2019).

27. Fujihira, E., Tamura, N. & Yamaguchi, A. Membrane topology of a multidrug efflux transporter, AcrB, in Escherichia coli. *J. Biochem.* **131**, 145–151 (2002).
28. Tikhonova, E. B., Wang, Q. & Zgurskaya, H. I. Chimeric analysis of the multicomponent multidrug efflux transporters from gram-negative bacteria. *J. Bacteriol.* **184**, 6499–6507 (2002).
29. Li, G. & Peter Howard, S. In Vivo and In Vitro Protein-Peptidoglycan Interactions. *Methods Mol. Biol.* **1615**, 143–149 (2017).
30. Mastronarde, D. N. SerialEM: A Program for Automated Tilt Series Acquisition on Tecnai Microscopes Using Prediction of Specimen Position. *Microscopy and Microanalysis* **9**, 1182–1183 (2003).
31. Bell, J. M., Chen, M., Baldwin, P. R. & Ludtke, S. J. High resolution single particle refinement in EMAN2.1. *Methods* **100**, 25–34 (2016).
32. Chen, M., Bell, J. M., Shi, X., Sun, S. Y., Wang, Z & Ludtke, S. J. A complete data processing workflow for CryoET and subtomogram averaging. Preprint at http://arXiv.org/abs/1902.03978 (2019).
33. Goddard, T. D., Huang, C. C. & Ferrin, T. E. Visualizing density maps with UCSF Chimera. *J. Struct. Biol.* **157**, 281–287 (2007).

Acknowledgements

This work was supported by the Welch Foundation (Q-1967-20180324), BCM BMB department seed funds, NIH R01GM080139 and P01GM121203. B.F.L. and D.D. are supported by an ERC Advanced Award. We thank X. Yu, T. Huo and H. Wu for helpful suggestions on sample preparation, MIC assay and initial model drawing; S. Raveendran for data backup. We thank Tim Opperman and colleagues for the kind gift of the AcrB inhibitor.

Author contributions

Z.W. designed the experiments; S.J.L. developed computational methods; X.S. and Z.Y. performed the experiments; B.F.L. performed the in vivo crosslinking experiments. M.C performed computational analyses; X.S., I.F., J.A. and H.V. screened samples and collected data; X.S., M.C., H.W., M.B. and Z.W. analyzed data; X.S., M.C. and Z.W. wrote the manuscript; D.D., B.F.L. and S.L. reviewed and edited the manuscript.

Competing Interests: The authors declare no competing interests.

Figures Legends

Figure 1 | Visualizing the AcrAB-TolC efflux pump in the *E. coli* cell envelope. (**a**) A single slice from a tomogram of *E. coli*. The condensed materials shown inside of the cell are inclusion bodies resulting from membrane protein overexpression. (**b**) Zoomed in side view of the cell envelope containing the AcrAB-TolC pump which is indicated by the red rectangle. (**c**) Corresponding three-dimensional annotation of b showing the outer membrane (OM; blue), the inner membrane (IM; blue), peptidoglycan (PG; yellow), and the AcrAB-TolC pump (cyan). (**d**) Top view of the cell envelope containing the AcrAB-TolC pumps which appear as ring-shaped densities (indicated by the red circle).

Figure 2 | In situ Cryo-ET structures of the fully assembled AcrAB-TolC complex. (**a**) The side-view projection of the subtomogram average of the pump in presence of antibiotics. (**b**) Isosurface rendering of a fitted with high resolution cryo-EM model (PDB: 5V5S). (**c**) A slice through b showing a constriction at the boundary between AcrA and TolC (indicated by the red arrow). (**d**) A slice through the density map of the pump in presence of AcrB inhibitor (MBX3132). (**e**) Isosurface rendering of b overlaid with density map of the cell envelope.

Figure 3 | In situ structure of the AcrAB subcomplex. (**a**) The side-view projection of the subtomogram average of the AcrAB subcomplex in presence of antibiotics. (**b**) Isosurface rendering of a fitted with the cryo-EM single-particle model (PDB: 5V5S). (**c**) A slice through the density map of b. (**d**) Isosurface rendering of b overlaid with density map of the cell envelope.

Figure 4 | Proposed in vivo assembly and functioning mechanism for multidrug efflux pump AcrAB-TolC. First, AcrB associates with AcrA to form the bipartite complex AcrAB. Next, AcrA changes its conformation to recruit TolC. Once TolC binds with the AcrAB bipartite complex, the fully assembled tripartite pump remains in the resting state. When AcrB encounters a drug molecule, the pump adopts an open conformation accompanied with a contraction along the long axis and the substrate is expelled through the channel and out of the cell.

413 **Figure 1**

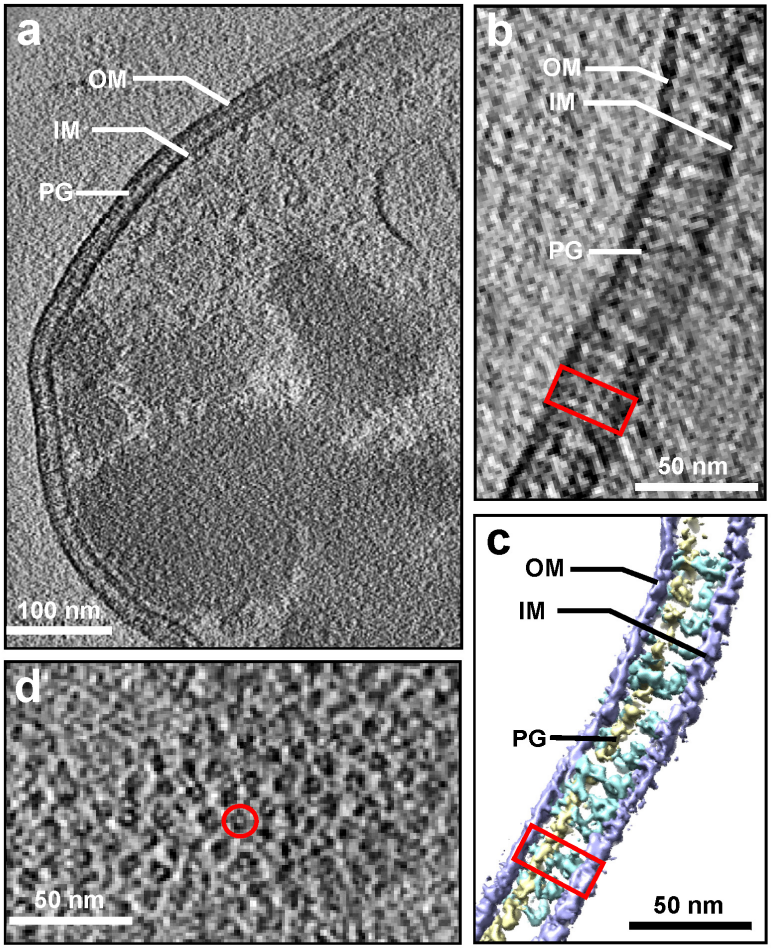

414

415 **Figure 2**

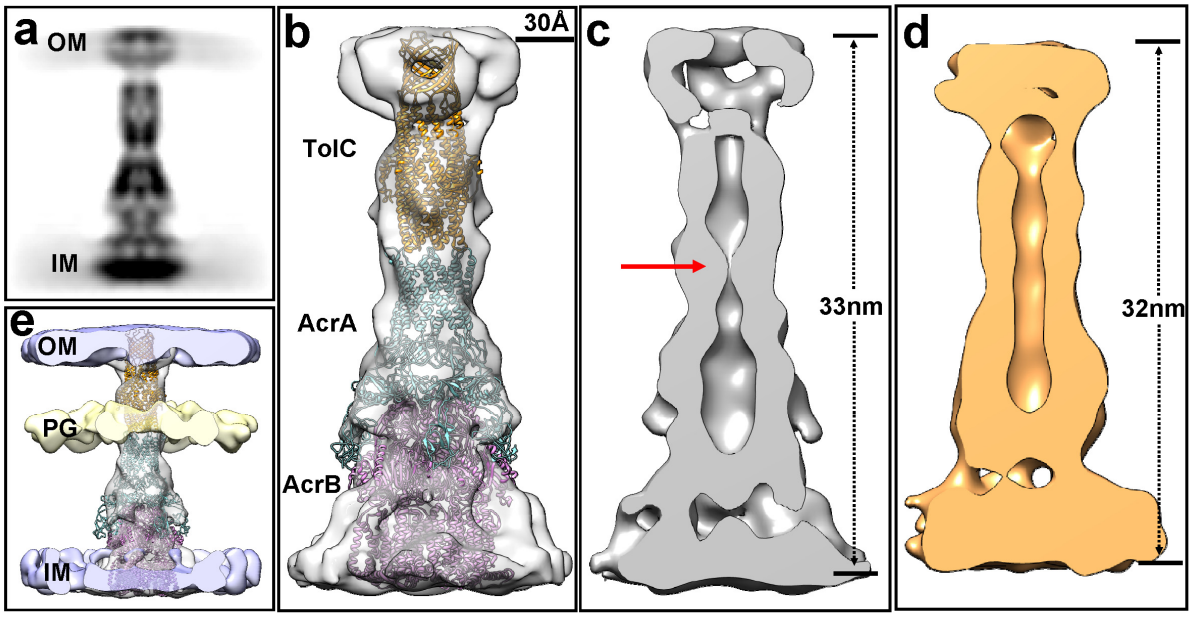

416

417 **Figure 3**

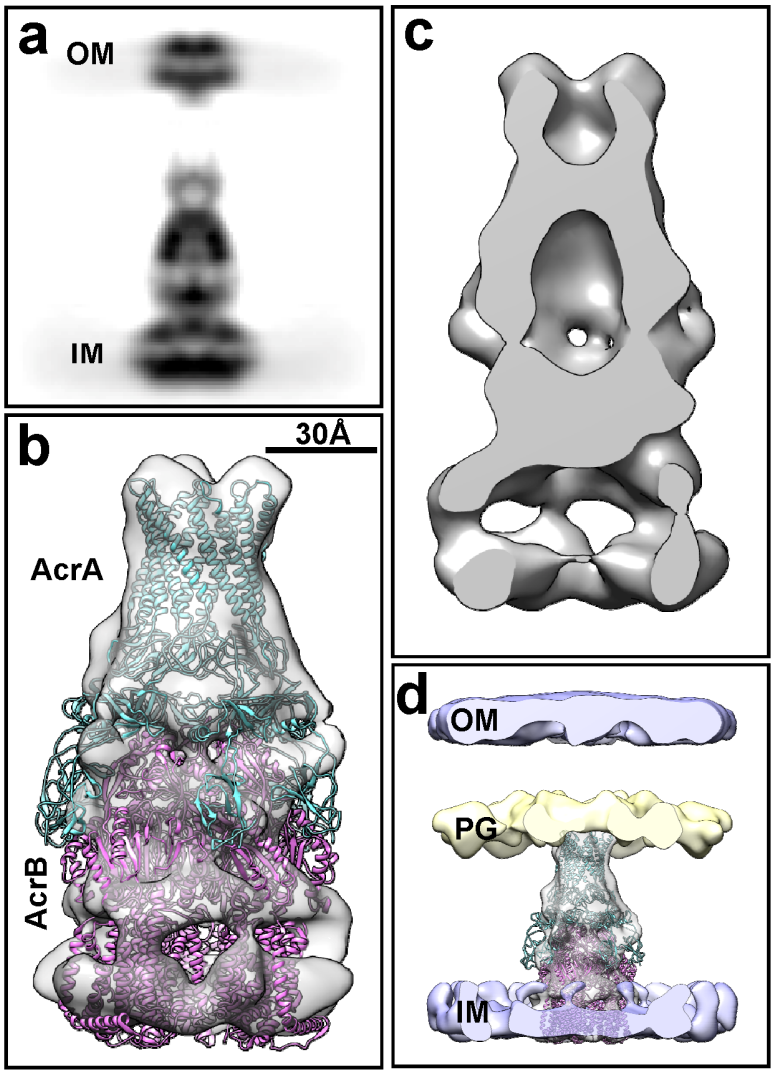

418

419 **Figure 4**

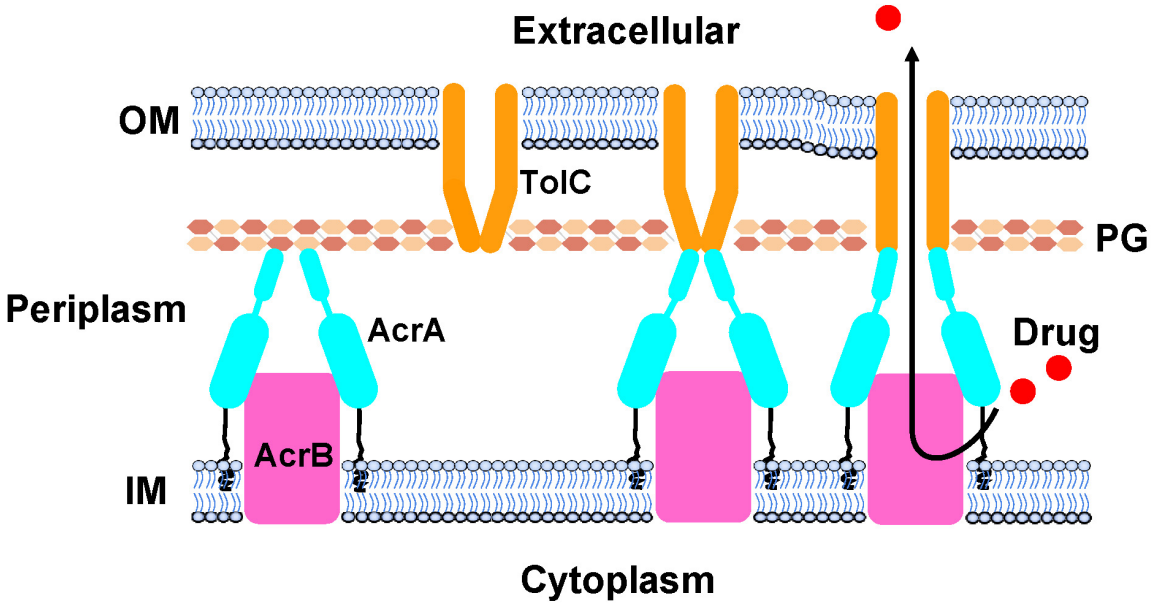

420

Supplementary Information for

Shi *et al.*'s manuscript entitled "In situ structure and assembly of multidrug efflux pump AcrAB-TolC"

Supplementary Figures and Tables

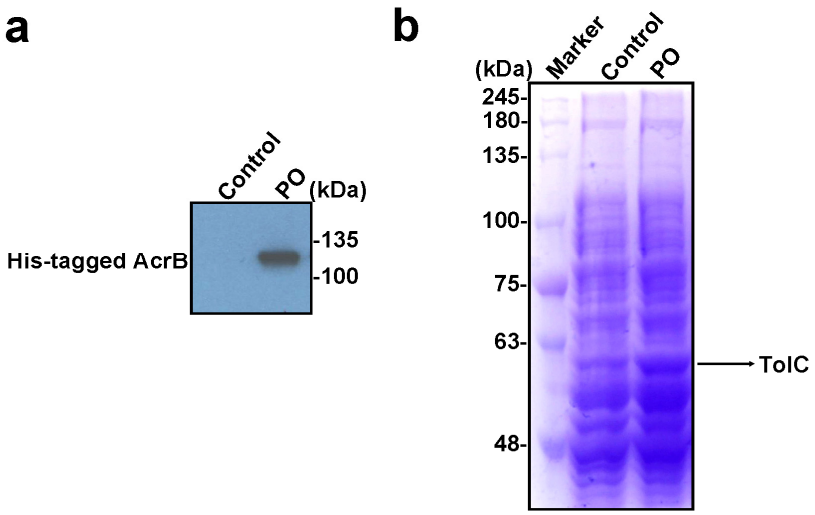

Supplementary Figure 1 | Overexpression of AcrA, AcrB, and TolC in BL21(DE3) cells. Expression plasmids pAcBH encoding AcrA and AcrB and pRSF-*tolC* were cotransformed into BL21 (DE3) cells. Protein expression was induced with 0.1 mM IPTG at 20 ^{o}C overnight. BL21 (DE3) cells without plasmid transformation were used as the control. (**a**) Immunoblotting results of AcrB overexpression by using anti-his antibodies. Source data are provided as a Source Data file. (**b**) SDS-PAGE analysis result of TolC overexpression. PO: pump overexpression.

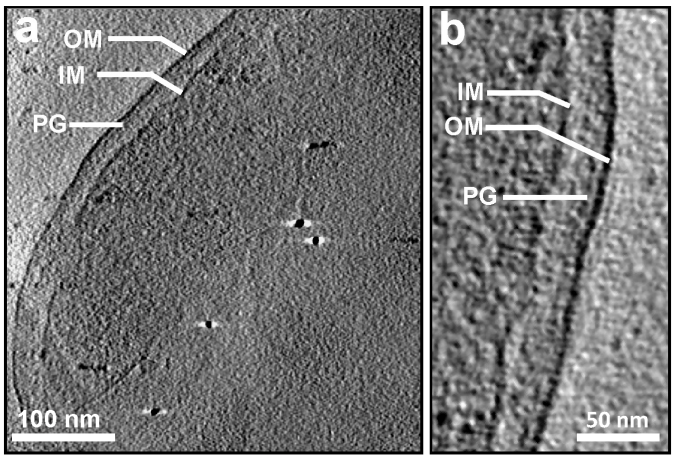

Supplementary Figure 2 | Visualizing the cell envelope of *E. coli* BL21 (DE3) wild type cells. (**a**) A single slice from a tomogram of *E. coli*. (**b**) Zoomed in side view of the cell envelope. OM, outer membrane; IM, inner membrane; PG, peptidoglycan.

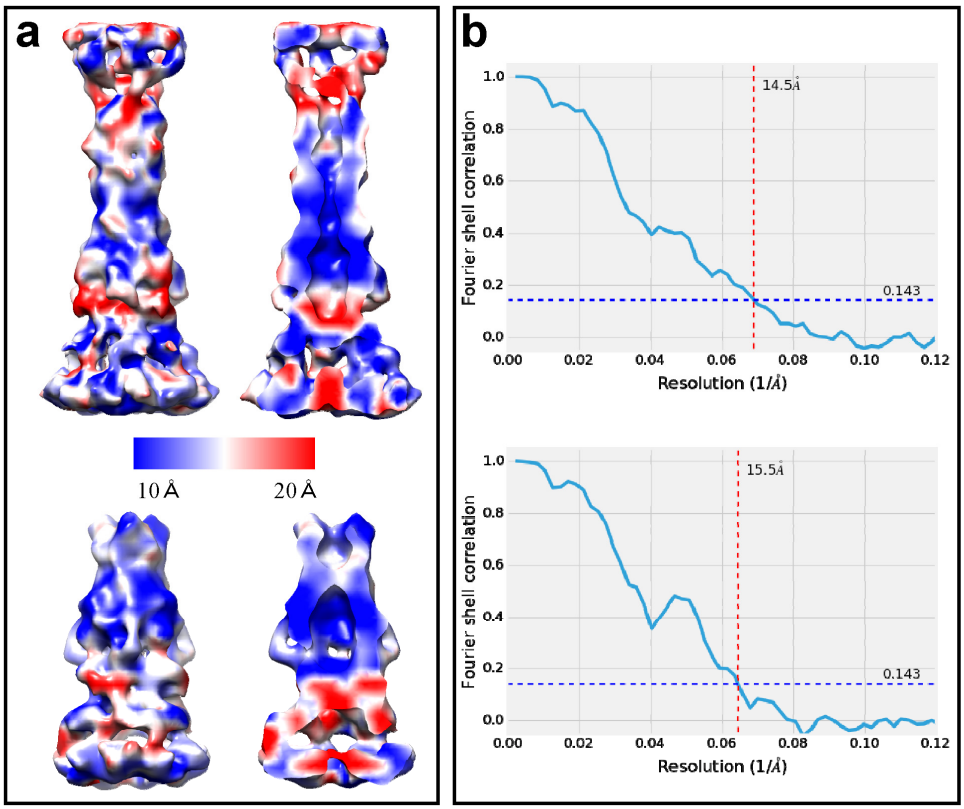

Supplementary Figure 3 | Local and global resolution of the subtomogram average. (**a**) Local resolution of the averaged structure overlaid on the isosurface rendering. Upper: full pump; lower: AcrAB subcomplex. (**b**) Global gold-standard FSC curve of the averaged structure under a soft mask. Upper: full pump; lower: AcrAB subcomplex.

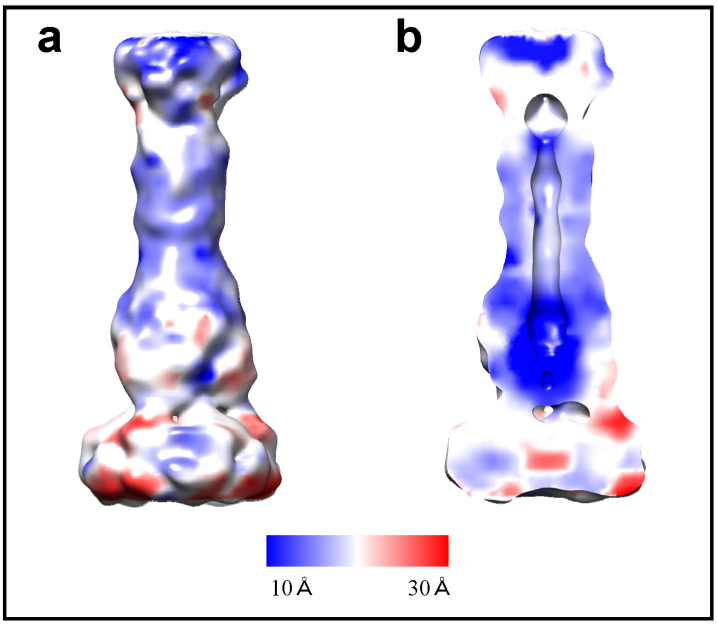

Supplementary Figure 4 | Local resolution of the subtomogram average of the fully assembled pump under inhibitor treatment. (**a**) Local resolution of the averaged structure overlaid on the isosurface rendering. (**b**) A slice through the density map of a.

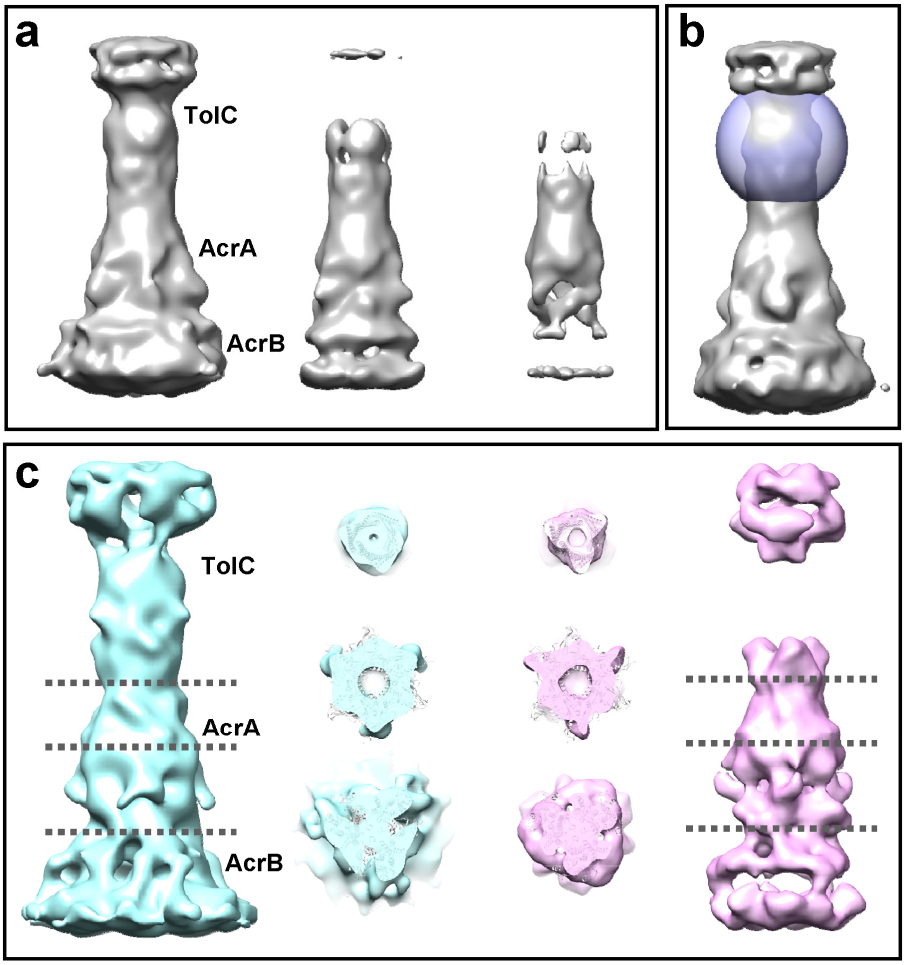

Supplementary Figure 5 | Focused classification to evaluate particle composition. (**a**) Reconstructions for the pump at different isosurface level (from left to right, with isosurface threshold increasing). (**b**) Mask for focused classification (blue) overlaid on the structure. (**c**) Cross section views of the averaged density maps from the two classes at the AcrA and AcrB subunit, fitted with the PDB model (5V5S). Cyan: fully assembled pump; pink: AcrAB subcomplex.

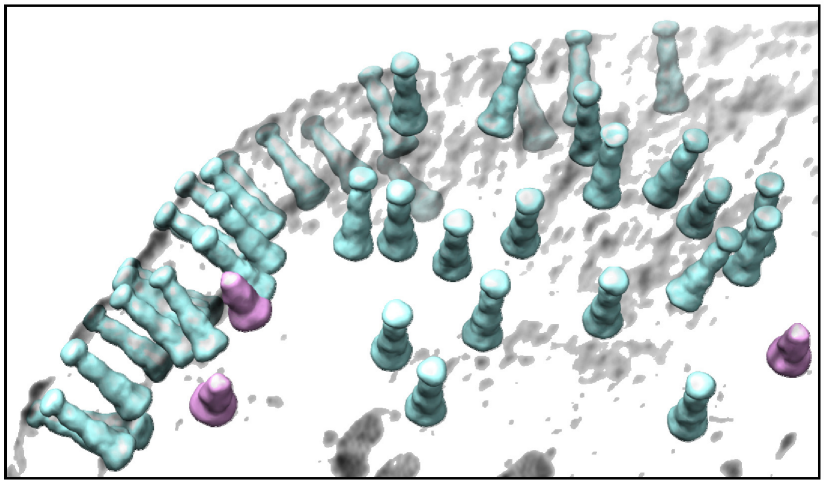

Supplementary Figure 6 | Segmentation showing fully assembled AcrAB-TolC pump and AcrAB subcomplex distributed in their original cell.

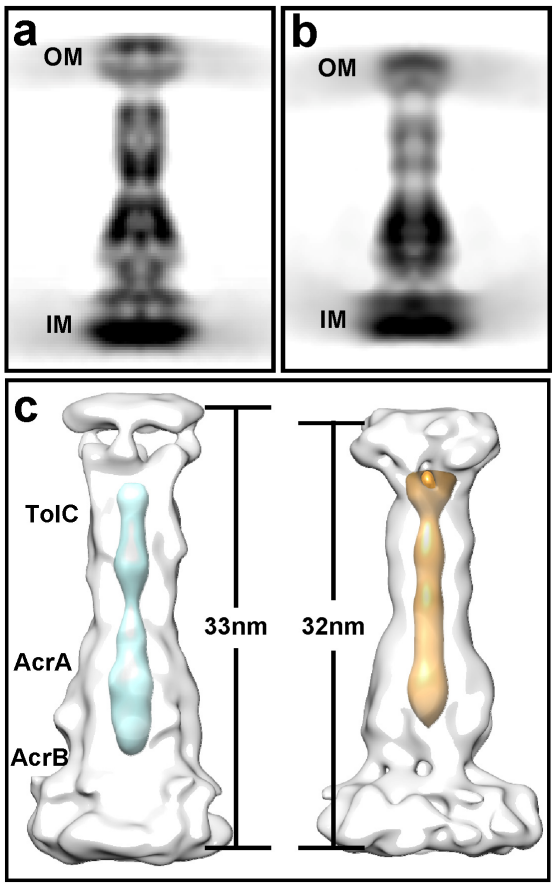

Supplementary Figure 7 | Comparison of the structure solved with antibiotics (closed state) treatment and with AcrB inhibitor (open state). (**a**) Projection of the full pump structure at closed state. (**b**) Projection of the full pump structure at open state. (**c**) Three-dimensional density maps of the closed (left) and open (right) state pump, both filtered to 21 Å, with the colored inner channel overlaid.

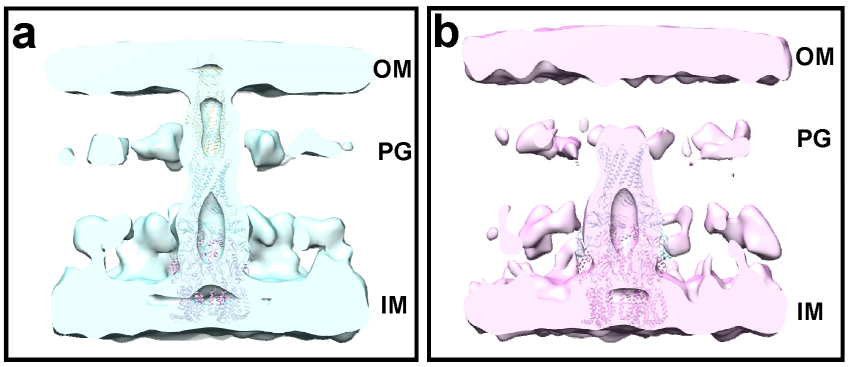

Supplementary Figure 8 | Reconstructions of AcrAB-TolC efflux pump in their surrounding environment. Density maps of the two classes refined without a mask fitted with the PDB model (5V5S), show the location of the peptidoglycan layer. (**a**) Fully assembled pump (cyan). (**b**) AcrAB subcomplex (pink).

a

3::sp|P02930|TOLC_ECOLI **Mass:** 53708 **Score:** 1389 **Matches:** 35(32) **Sequences:** 25(24) **emPAI:** 11.12
Outer membrane protein TolC OS=Escherichia coli (strain K12) OX=83333 GN=tolC PE=1 SV=3
Check to include this hit in error tolerant search or archive report

Query	Observed	Mr(expt)	Mr(calc)	ppm	Miss	Score	Expect	Rank	Unique	Peptide
1653	559.3140	1116.6135	1116.6139	-0.33	0	54	6.2e-05	1	U	Y.KQAVVSAQSSL.D
1728	566.7918	1131.5691	1131.5706	-1.34	0	(25)	0.092	1	U	L.KEAEKRNL.S + DTSSP_Cross_link_Carbamidomethyl (K)
1861	578.8193	1155.6241	1155.6247	-0.53	0	46	0.00032	1	U	F.EKINEARSPL.L
1886	580.3356	1158.6566	1158.6609	-3.69	0	24	0.043	1	U	Y.SVGTRTIVDVL.D
2230	605.8430	1209.6715	1209.6717	-0.19	0	48	0.0001	1	U	F.KTDKPQFVNAL.L
2486	415.8922	1244.6547	1244.6546	0.05	1	26	0.053	1	U	L.LKEAEKRNL.S + DTSSP_Cross_link_Carbamidomethyl (K)
2687	639.2931	1276.5717	1276.5718	-0.01	0	(32)	0.022	1	U	Y.DDSNMGQNKVGL.S
2688	639.3015	1276.5883	1276.5903	-1.55	0	34	0.015	1	U	L.KEAEKRNL.S + 2 DTSSP_Cross_link_Carbamidomethyl (K)
2692	639.3332	1276.6518	1276.6523	-0.40	1	47	0.00065	1	U	Y.NAKQELANARY.N
2822	647.2885	1292.5625	1292.5667	-3.26	0	50	0.00023	1	U	Y.DDSNMGQNKVGL.S + Oxidation (M)
2877	651.3222	1300.6298	1300.6299	-0.04	1	35	0.01	1	U	L.SYTQAQKEAIY.R
3035	661.8308	1321.6471	1321.6514	-3.26	0	22	0.31	1	U	L.QEKAAGIQDVTY.Q
3048	662.3846	1322.7547	1322.7558	-0.80	1	51	3.4e-05	1	U	F.KTDKPQFVNALL.K
3435	690.8448	1379.6751	1379.6681	5.14	0	43	0.0025	1	U	F.NNINASISSINAY.K
3862	724.8793	1447.7440	1447.7419	1.42	0	92	2.5e-08	1	U	L.VAITDVQNARAQY.D
3972	734.8949	1467.7752	1467.7755	-0.19	1	(37)	0.0035	1	U	F.KTDKPQFVNALL.K + DTSSP_Cross_link_Carbamidomethyl (K)
3975	735.3501	1468.6856	1468.6868	-0.76	2	32	0.036	1	U	F.SSLSQAENLMQVY.Q
4112	746.3549	1490.6953	1490.6961	-0.53	0	79	6.7e-07	1	U	Y.RDANGINSNATSASL.Q + Deamidated (NQ)
4113	746.3575	1490.7004	1490.6961	2.91	0	(37)	0.011	1	U	Y.RDANGINSNATSASL.Q + Deamidated (NQ)
4341	768.8980	1535.7813	1535.7831	-1.16	1	78	6.7e-07	1	U	L.TLQEKAAGIQDVTY.Q
4342	769.3738	1536.7330	1536.7355	-1.60	0	(59)	7.4e-05	1	U	Y.QGGMVNSQVKQAQY.N
4418	777.3720	1552.7295	1552.7304	-0.60	0	62	4.6e-05	1	U	Y.QGGMVNSQVKQAQY.N + Oxidation (M)
4693	804.9236	1607.8327	1607.8307	1.26	2	40	0.0036	1	U	L.RQITGNYYPELAAL.N
5577	881.4841	1760.9536	1760.9520	0.89	1	72	1.1e-06	1	U	Y.SVGTRTIVDVLDATTTL.Y
5842	916.4874	1830.9603	1830.9588	0.82	1	127	6e-12	1	U	F.NVGLVAITDVQNARAQY.D
5843	611.3275	1830.9607	1830.9588	1.04	1	(62)	1.9e-05	1	U	F.NVGLVAITDVQNARAQY.D
5919	927.9475	1853.8805	1853.8829	-1.31	1	91	6.6e-08	1	U	Y.KQAVVSAQSSLDAMEAGY.S
5979	935.9656	1869.9167	1869.9180	-0.70	1	66	1.6e-05	1	U	L.ANEVTARNNLDNAVEQL.R
6138	963.0156	1924.0166	1924.0153	0.63	2	57	5e-05	1	U	Y.SVGTRTIVDVLDATTTLY.N
6364	1000.4556	1998.8966	1998.9026	-3.03	1	(71)	6.4e-06	1	U	Y.KQAVVSAQSSLDAMEAGY.S + DTSSP_Cross_link_Carbamidomethyl (K)
7088	1150.0791	2298.1436	2298.1451	-0.65	2	67	1.4e-05	1	U	Y.DTVLANEVTARNNLDNAVEQL.R
7093	767.3895	2299.1468	2299.1292	7.66	2	(23)	0.33	1	U	Y.DTVLANEVTARNNLDNAVEQL.R + Deamidated (NQ)
7456	636.3040	2541.1867	2541.1878	-0.41	1	(36)	0.028	1	U	Y.SGSKTRGAAGTQYDDSNMGQNKVGL.S
7471	640.3030	2557.1831	2557.1827	0.14	1	56	0.00029	1	U	Y.SGSKTRGAAGTQYDDSNMGQNKVGL.S + Oxidation (M)
7472	853.4025	2557.1856	2557.1827	1.13	1	(41)	0.0084	1	U	Y.SGSKTRGAAGTQYDDSNMGQNKVGL.S + Oxidation (M)

b

4::sp|P0AE06|ACRA_ECOLI **Mass:** 42301 **Score:** 767 **Matches:** 32(29) **Sequences:** 16(14) **emPAI:** 10.09
Multidrug efflux pump subunit AcrA OS=Escherichia coli (strain K12) OX=83333 GN=acrA PE=1 SV=1
Check to include this hit in error tolerant search or archive report

Query	Observed	Mr(expt)	Mr(calc)	ppm	Miss	Score	Expect	Rank	Unique	Peptide
857	487.2687	972.5229	972.5240	-1.09	1	26	0.041	1	U	L.KQELANGTL.K
1640	557.8320	1113.6494	1113.6506	-1.09	0	49	9.6e-05	1	U	L.KAGDRVVISGL.Q
2456	621.8619	1241.7092	1241.7092	0.05	2	(41)	0.00069	1	U	L.RLKQELANGTL.K
2467	622.3532	1242.6919	1242.6932	-1.04	2	(47)	0.00023	1	U	L.RLKQELANGTL.K + Deamidated (NQ)
3347	684.3378	1366.6611	1366.6616	-0.36	1	67	9.7e-06	1	U	F.KEGSDIEAGVSLY.Q
3477	694.3727	1386.7308	1386.7289	1.38	2	50	0.00029	1	U	L.RLKQELANGTL.K + DTSSP_Cross_link_Carbamidomethyl (K)
4120	746.3862	1490.7579	1490.7617	-2.54	0	40	0.0043	1	U	L.ITSDGIKFPQDGTL.E
4407	775.9718	1549.9290	1549.9304	-0.87	0	31	0.00079	1	U	Y.RIAEVRPQVSGIIL.K
4409	517.6504	1549.9293	1549.9304	-0.68	0	(22)	0.0065	1	U	Y.RIAEVRPQVSGIIL.K
5606	884.4441	1766.8736	1766.8727	0.53	1	33	0.03	1	U	L.ITSDGIKFPQDGTLEF.S
5664	893.4141	1784.8136	1784.8139	-0.18	1	24	0.32	1	U	L.EFSDVTVDQTTGCITL.R
5818	609.3182	1824.9327	1824.9345	-0.98	1	(42)	0.0026	1	U	L.RAIFPNPDHTLLPGMF.V
5819	913.4756	1824.9366	1824.9345	1.16	1	(36)	0.011	1	U	L.RAIFPNPDHTLLPGMF.V
5881	614.6508	1840.9305	1840.9294	0.56	1	48	0.00077	1	U	L.RAIFPNPDHTLLPGMF.V + Oxidation (M)
5882	921.4742	1840.9339	1840.9294	2.44	1	(40)	0.0041	1	U	L.RAIFPNPDHTLLPGMF.V + Oxidation (M)
5924	928.4946	1854.9747	1854.9799	-2.79	1	78	3.5e-07	1	U	Y.DSAKGDLAKAQAAANIAQL.T
5925	619.3334	1854.9785	1854.9799	-0.75	1	(63)	1.1e-05	1	U	Y.DSAKGDLAKAQAAANIAQL.T
6373	1001.0056	1999.9967	1999.9996	-1.47	1	(57)	0.0001	1	U	Y.DSAKGDLAKAQAAANIAQL.T + DTSSP_Cross_link_Carbamidomethyl (K)
7348	818.7704	2453.2893	2453.2914	-0.86	0	46	0.00067	1	U	L.VVGADDKVETRPIVASQAIGDKW.L
7521	867.1120	2598.3142	2598.3112	1.15	0	(45)	0.0016	1	U	L.VVGADDKVETRPIVASQAIGDKW.L + DTSSP_Cross_link_Carbamidomethyl (K)
7625	892.1520	2673.4341	2673.4337	0.14	1	67	3.5e-06	1	U	L.KQENGKAKVSLITSDGIKFPQDGTL.E
7626	669.3658	2673.4343	2673.4337	0.20	1	(46)	0.00046	1	U	L.KQENGKAKVSLITSDGIKFPQDGTL.E
7627	535.6952	2673.4396	2673.4337	2.18	1	(28)	0.027	1	U	L.KQENGKAKVSLITSDGIKFPQDGTL.E
7770	932.4926	2794.4558	2794.4573	-0.52	1	53	0.00015	1	U	Y.DQALADAQQANAAVTAAKAAVETARINL.A
7883	981.4824	2941.4253	2941.4274	-0.73	0	70	1.1e-05	1	U	L.TGCDDKQAQQGGQQMPAVGVVTVKTEPL.Q
8060	1048.5520	3142.6342	3142.6292	1.58	1	20	0.3	1	U	Y.TKVTSPISGRIGKSNVTEGALVQNGQATAL.A + Deamidated (NQ); DTSSP_Cross_link_Carbamidomethyl (K)
8224	696.5585	3477.7563	3477.7560	0.07	0	(33)	0.028	1	U	L.QKVRPGVQVKAQEVTADNNQQAASGAQPEQSKS.-
8225	870.4464	3477.7565	3477.7560	0.15	0	68	9.8e-06	1	U	L.QKVRPGVQVKAQEVTADNNQQAASGAQPEQSKS.-
8227	696.7571	3478.7493	3478.7400	2.67	0	(39)	0.0079	1	U	L.QKVRPGVQVKAQEVTADNNQQAASGAQPEQSKS.- + Deamidated (NQ)
8262	906.7007	3622.7736	3622.7758	-0.59	0	(33)	0.042	1	U	L.QKVRPGVQVKAQEVTADNNQQAASGAQPEQSKS.- + DTSSP_Cross_link_Carbamidomethyl (K)
8263	906.7020	3622.7789	3622.7758	0.87	0	(27)	0.18	1	U	L.QKVRPGVQVKAQEVTADNNQQAASGAQPEQSKS.- + DTSSP_Cross_link_Carbamidomethyl (K)
8265	907.2026	3624.7815	3624.7438	10.4	0	(48)	0.0013	1	U	L.QKVRPGVQVKAQEVTADNNQQAASGAQPEQSKS.- + 2 Deamidated (NQ); DTSSP_Cross_link_Carbamidomethyl (K)

Supplementary Figure 9 | Crosslinking of AcrA and TolC with PG in vivo as detected by LC/MS-MS analysis. (**a**) The MASCOT output for peptides from TolC for the SDS-PAGE extracted sample. (**b**) The MASCOT output for peptides from AcrA for SDS-PAGE extracted sample.

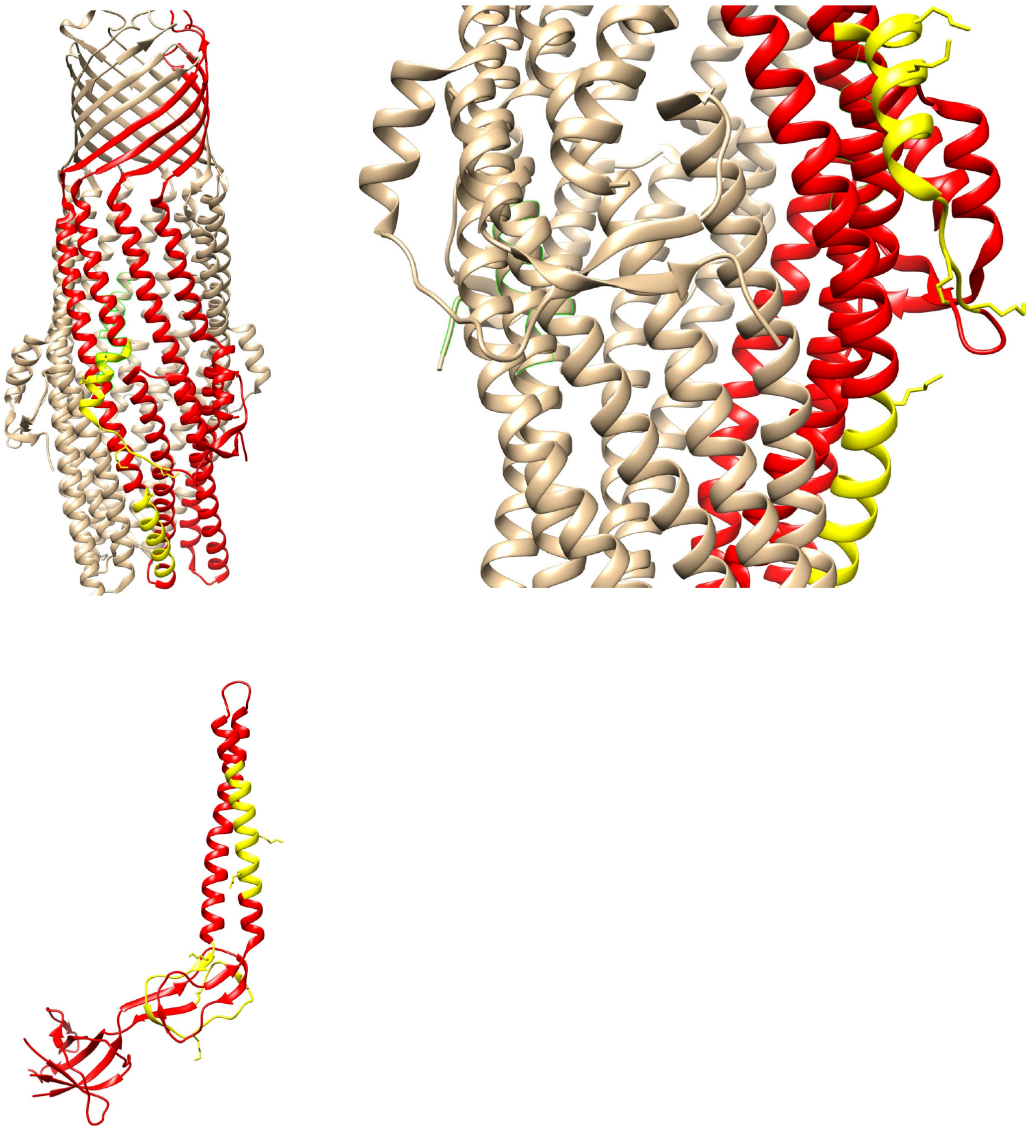

Supplementary Figure 10 | Mapping the binding sites of both AcrA and TolC with PG. The crystal structures of TolC trimer (upper panel, PDB: 1EK9) and AcrA (lower panel, PDB: 2F1M) with mapped peptides, highlighted in yellow. The candidate lysine residues that interact with the DTSSP bifunctional crosslinker are shown with side chains (K202, K205, K214, K218, K345 for TolC; K109, K114 in AcrA helical hairpin and K175, K186 in AcrA lipoyl domain). The right panels show zoomed views. For clarity, the mapped peptides are shown for only one protomer of the TolC trimer. The figures were prepared with UCSF Chimera.

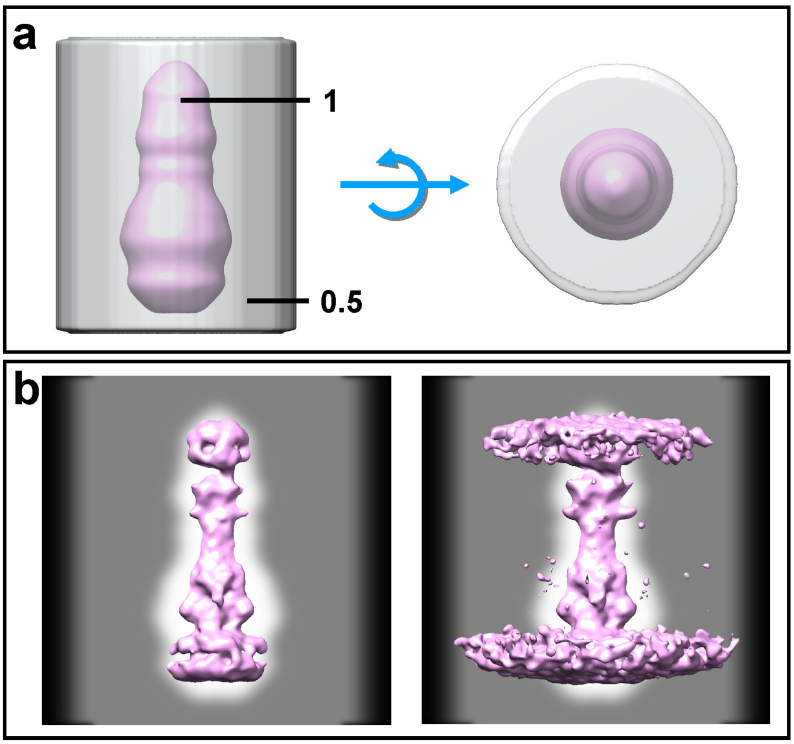

Supplementary Figure 11 | Masking strategy. (a) Top and side view of the two-level mask used for refinement. The pink density in the middle has the value of 1 and the grey density around has the value of 0.5. A soft falloff was applied at the interface between the pink and grey density, and at the edge of the grey density. (**b**) Two-dimensional slice of the mask in the X-Z direction and the averaged map at high and low isosurface threshold.

Supplementary Table 1 | Puromycin susceptibility of *E. coli* BL21 (DE3) cells over-expressing AcrAB-TolC pump.

Proteins expressed	MIC (μg/ml)	
	In the absence of MBX3132	In the presence of MBX3132 (1.4 μg/ml)
-	32	8
AcrA, AcrB, TolC	64-128	8

Supplementary Table 2 | Cryo-ET data analysis and validation statistics.

	AcrAB-TolC open state (EMD-0533)	AcrAB-TolC close state (EMD-0532)	AcrAB subcomplex (EMD-0531)
Data collection and processing			
Magnification	12,000	10,000	10,000
Voltage (kV)	300	300	300
Electron exposure (e–/Å^2)	76	76	76
Defocus range (μm)	−3 to−6	−3 to−6	−3 to−6
Pixel size (Å)	2.75	3.366	3.366
Symmetry imposed	C3	C3	C3
Initial particle images (no.)	678	1,321	1,321
Final particle images (no.)	678	800	561
Map resolution (Å)	21	15	15
FSC threshold	0.143	0.143	0.143
Map resolution range (Å)	10-30	10-20	10-20